Computers and Geotechnics 90 (2017) 155–163

Contents lists available at ScienceDirect

Computers and Geotechnics

journal homepage: www.elsevier.com/locate/compgeo

Research Paper

# An axisymmetric BNEF method of circular excavations taking into account soil-structure interactions

Wei He [a,*], Chaoyun Luo [b], Jianfeng Cui [c], Jianren Zhang [a]

[a] Changsha University of Science & Technology, Changsha, Hunan, China
[b] Guangdong Provincial Changda Highway Engineering Co., Ltd., Guangzhou, Guangdong, China
[c] Hunan Provincial Communications Planning, Survey, & Design Institute, Changsha, Hunan, China

ARTICLE INFO

*Article history:*
Received 12 October 2016
Received in revised form 26 April 2017
Accepted 5 June 2017

*Keywords:*
Circular excavation
Cylinder diaphragm wall
Ring beam
BNEF method
Soil-structure interaction

ABSTRACT

An axisymmetric BNEF method was proposed to analyze circular excavations. The governing equations of embedded cylindrical diaphragm walls were derived from thin-shell theory. A hyperbolic model was proposed to account for soil-structure interactions. Then, a FEM program was coded and verified using a case study. Overall, the method caught the main trend in the measured results and provided a reasonable estimation for engineering practice. Furthermore, the development of earth pressure and the hoop stress in the walls (ring beams) can be obtained using conventional parameters, extending the ability of the classic BEF method to aid the design of circular excavations.



## 1. Introduction

Circular excavation is preferred in soft ground conditions. Due to the so-called hoop effect, this type of excavation is advantageous to achieve less wall deflection, smaller internal force, and higher stability of retaining structures, usually diaphragm walls. Field measurements indicated remarkably less wall deflection when adopting circular excavation [1,2]. However, it is crucial to reasonably model circular excavation to ensure an economical design.

The key to circular excavation modelling is taking the hoop effect into account. The 3D and 2D axisymmetric methods are capable of considering this effect, and the latter is most common in engineering practice. Cabarkapa designed a 56.6 m diameter, 28 m deep circular TBM launch and reception shaft with a 2D axisymmetric finite element model, and the measured wall displacements were compared to the calculated values [3]. Mcnamara developed an 8.2 m diameter, 40 m deep shaft with an axisymmetric analysis [4]. Schwamb reported a comprehensive numerical analysis performed using the commercially available software Flac2D [5]. The influence factors, such as the anisotropy of the diaphragm walls, panel installation effects, and advanced soil models, were studied. In addition to the 2D axisymmetric method, circular excavation can also be simplified as a beam-on-elastic-foundation (BEF) model, which is more practical and user friendly [6]. Tan reported a deep circular excavation design using this method, and the calculated result agreed well with the measured result [7]. However, in the design, the sizes of waler beams were determined based on local experience, which could not be accounted for in the model. Therefore, it is necessary to enhance the ability of the BEF method to aid engineering design.

Furthermore, the BEF method has great potential to be incorporated into reliability analysis, which is important for assessing the risk level of a project [8–10]. In this paper, an axisymmetric beam on a nonlinear elastic foundation (BNEF) method was proposed based on thin-shell theory, taking into account the nonlinear characteristics of soil-structure interactions and overburden stress release due to soil pit. Exhaustive calculation results, including the hoop stress in the walls and ring beams, can be obtained for design purposes.

## 2. The axisymmetric BNEF method

### 2.1. Governing equations of an embedded thin shell

Fig. 1 shows a typical circular excavation retaining system for the anchorage of a suspension bridge, which includes several wall panels and ring beams installed after each layer of soil pit. For general scenarios, the following basic assumptions were introduced to simplify the model,

* Corresponding author.
*E-mail address:* wadeho@icloud.com (W. He).

http://dx.doi.org/10.1016/j.compgeo.2017.06.001
0266-352X/

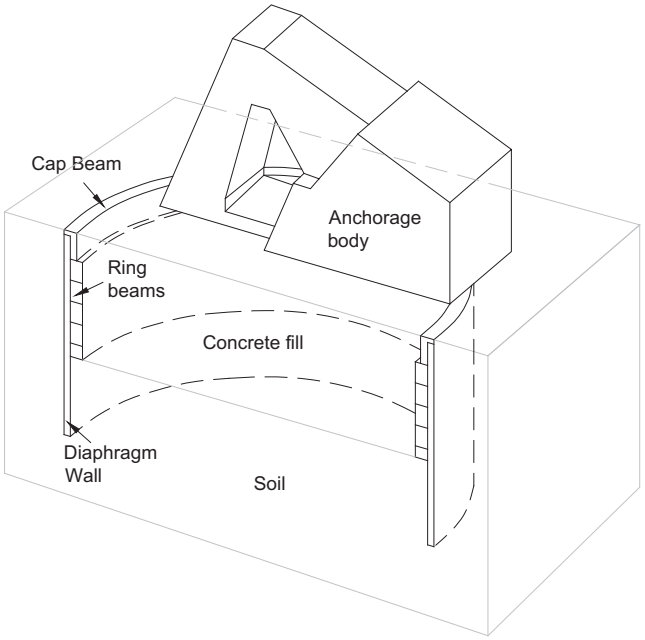


**Fig. 1.** A typical retaining structure for the circular excavation of a suspension bridge anchorage.

- Assume axisymmetrical retaining structures, surrounding soil stratum, construction sequences, and external forces in a circular excavation;
- Both sides of the diaphragm wall panels are connected to nonlinear soil springs, with an initial stress of the at-rest earth pressure;
- Diaphragm wall panels are anisotropic due to the joints between the initial panels and sequential panels.

Under these assumptions, a cylindrical retaining structure can be idealized as an embedded thin shell as the ratio of the wall thickness to radius is less than 1/20 for most deep circular excavations.

The internal forces of an embedded thin shell under external force $q$ are shown in Fig. 2, where $T$ denotes shear forces, $N$ denotes axial forces, $M$ denotes moments, and the subscripts, $r, \phi$, and $z$ are the radial, circumferential, and vertical directions in the cylindrical coordinate system, respectively. The adopted sign convention is that stress/strain are positive in compression. For an embedded cylindrical thin shell, $\frac{h^2}{R^2}$ in the Timoshenko equations [11] can be neglected. Then, with soil springs introduced, we obtain:

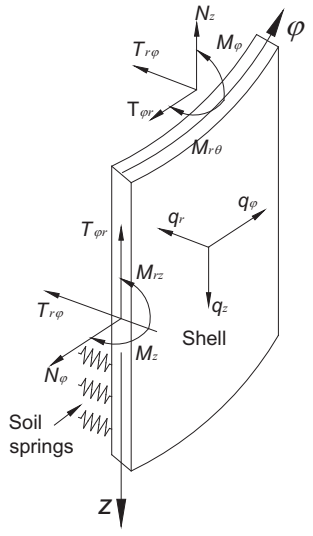


**Fig. 2.** Internal forces in an embedded cylindrical shell.

$$\left.\begin{aligned}
&\left(\frac{\partial^2}{\partial z^2}+\frac{1-\nu}{2R^2}\frac{\partial^2}{\partial\varphi^2}\right)u_z+\left(\frac{1+\nu}{2R}\frac{\partial^2}{\partial z\partial\phi}\right)u_\phi-\left(\frac{\nu}{R}\frac{\partial}{\partial z}\right)u_r=0\\
&\left(\frac{1+\nu}{2R}\frac{\partial^2}{\partial z\partial\phi}\right)u_z+\left(\frac{1-\nu}{2}\frac{\partial^2}{\partial z^2}+\frac{1}{R^2}\frac{\partial^2}{\partial\phi^2}\right)u_\phi-\frac{1}{R^2}\frac{\partial}{\partial\phi}u_r=0\\
&\left(\frac{\nu}{R}\frac{\partial}{\partial z}\right)u_z+\frac{1}{R^2}\frac{\partial}{\partial\phi}u_\phi-\left(\frac{h^2}{12}\nabla^4+\frac{1}{R^2}+k(u_r)\right)u_r+\frac{1-\nu^2}{Eh}q_r=0
\end{aligned}\right\} \quad (1)$$

where $u_r, u_\phi$, and $u_z$ are the displacements along the radial, circumferential, and vertical directions in a cylindrical coordinate system, respectively; $\nu$ is the Poisson's ratio; $R$ is the radius of a circular excavation; $h$ is the wall thickness; and $k(u_r)$ is the stiffness of the soil springs.

Due to the axisymmetric assumptions, $u_\phi = 0, \frac{\partial}{\partial\phi} = 0$, and $q_z = 0$. Further, by neglecting the self weight of the retaining structures, the first equation of (1) yields:

$$\frac{\partial u_z}{\partial z}-\frac{\nu}{R}u_r=0 \quad (2)$$

Substituting Eq. (2) into the third equation of (1) and taking into account the anisotropy of the panels, we obtain:

$$DI\nabla^4 u_r+\frac{E_h h}{R^2}u_r+k(u_r)u_r=q_r \quad (3)$$

where $D$ is the flexural rigidity of a shell, and $D=\frac{E}{1-\nu^2}$; $E$ is the vertical elastic modulus of the diaphragm walls; $E_h$ is the circumferential elastic modulus; and $I$ is the moment of inertia.

Eq. (3) is the governing differential equation of an embedded anisotropic cylindrical diaphragm wall, in which $\frac{E_c h}{R^2}u_r$ brings in the hoop effect and panel anisotropy. The equation also indicates that for circular excavations, the vertical elastic modulus should be multiplied by $\frac{1}{1-\nu^2}$, which is 1.042 when $\nu = 0.2$.

According to thin-shell theory, the hoop stress, $\sigma_h$, in a diaphragm wall panel can be computed using:

$$\sigma_h=\frac{E_h}{R}u_r=\frac{\eta E}{R}u_r \quad (4)$$

where $\eta$ is the stiffness reduction coefficient.

### 2.2. Anisotropy of diaphragm walls

Two types of panels are commonly used in the construction of cylindrical diaphragm walls: initial panels with widths ranging from 6.1 m to 7.5 m and subsequent panels with widths of approximately 2.8 m. The weaker joints between wall panels lead to anisotropy in the diaphragm wall [12]. However, no agreement has previously been reached on the extent of the stiffness reduction. The stiffness reduction coefficient is recommended in the range of 0.4–0.7 based on consulting experience from France, and this range is adopted in Chinese code (JTJ D63-2007) [13] without further details. A set of experiments was designed and implemented to study the coefficient.

A group of 150 mm cubic specimens (Group A) containing joints were compressed, and their measured stiffnesses were compared to those of intact specimens (Group B). The joint width was set to 3 mm according to diaphragm wall construction experience in Japan [13]. The loading method in BS 1881-116 [14] was adopted. Fig. 3 shows the stress-strain relationship of the joints obtained from the measured data, in which T1, T2, and T3 denote three parallel testing results of Group A compared to the average stiffness of intact specimens in Group B. The results can be fitted by a broken line, and the mathematic formula is:

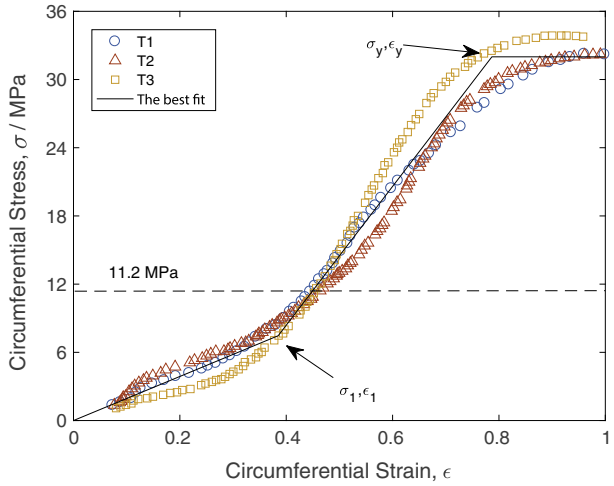


**Fig. 3.** The stress-strain relationship of the joints.

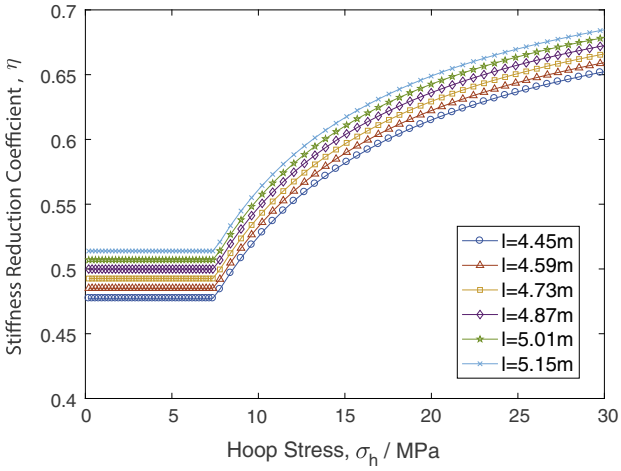


**Fig. 4.** The stiffness reduction coefficient vs. the hoop stress.

$$\sigma = \begin{cases} k_1\varepsilon & (\varepsilon \leqslant \varepsilon_1) \\ k_2(\varepsilon-\varepsilon_1)+k_1\varepsilon_1 & (\varepsilon_1 < \varepsilon \leqslant \varepsilon_y) \\ \sigma_y & (\varepsilon > \varepsilon_y) \end{cases} \tag{5}$$

where $\sigma$ and $\varepsilon$ are the stress and strain of the joints; $k_1$ and $k_2$ are the slopes of the 1st and 2nd Sections (19.39 MPa and 61.06 MPa in this tests), respectively; $\varepsilon_1$ and $\varepsilon_y$ are the characteristic strains separating the three sections (0.38 and 0.79 in this test); and $\sigma_y$ is the yield stress, 32 MPa.

The compression, $\delta_h$, of a ring can be computed by:

$$\delta_h = \frac{\sigma_h}{\bar{E}} 2r\pi \tag{6}$$

where $\delta_h$ is the compression; $\sigma_h$ is the hoop stress; and $\bar{E}$ is the equivalent Young's modulus of the walls.

Assume that the hoop stress in a wall is $\sigma_h$, the concrete elastic modulus is $E_c$, the stiffness of the joint is $E_j$, the average width of the wall is $w$, and the number of joints along the wall is $n$; then, the compression of a ring containing joints is:

$$\delta_h = \frac{\sigma_h}{E_c}(2r\pi - nw) + \frac{\sigma_h}{E_j} nw \approx \frac{\sigma_h}{E_c} 2r\pi + \frac{\sigma_h}{E_j} nw \tag{7}$$

Combining Eqs. (6) and (7) yields:

$$\eta = \frac{\bar{E}}{E_c} = \frac{1}{1+\frac{nw}{2r\pi}\frac{E_c}{E_j}} \tag{8}$$

The hydrofraises of 2.8 m in width is commonly applied in engineering practice, so the width of the subsequent panels is 2.8 m. Initial panels are commonly trenched with 3 cuttings, which leads to a width of 6.1–7.5 m. Hence, the average width of the panels, $l$, ranges from 4.45 m to 5.15 m. For different $l$, the relationship between the stiffness reduction coefficient, $\eta$, and the hoop stress, $\sigma_h$, can be computed using Eq. (8), as illustrated in Fig. 4. The coefficients remain constant until the hoop stress reaches 7.3 MPa, with a value ranging from 0.485 to 0.514, and increase nonlinearly thereafter. Fig. 4 also indicates that the shorter the average panel width is, the lower the stiffness reduction coefficient.

Without introducing the stiffness reduction coefficient, the BNEF method underestimates the deflection of the diaphragm wall panels. Therefore, when there is a lack of experience in a specific deep circular excavation, we recommend implementing the test presented in this paper to obtain the stiffness reduction coefficient. The concrete used in the tests is expected to be sampled at the site, while the width of joints is determined based on panel-construction experience.

### 2.3. The soil-structure interaction model

#### 2.3.1. Model description

There is a specific requirement for deep circular excavations to take soil-structure interaction effects into consideration as earth pressures hardly reach the limit value due to small wall displacements. Thus, both sides of a diaphragm wall should be connected to soil springs, as shown in Fig. 5(a).

Many experimental studies have indicated that earth pressure on a structure increases with displacement in a hyperbolic form [15–18]. Duncan et al. proposed a hyperbolic model for passive earth pressure as follows:

$$p = \frac{u}{\frac{1}{k_i} + \lambda\frac{u}{p_u}} \tag{9}$$

where $u$ is the radial displacement of a diaphragm wall; $k_i$ is the initial stiffness of a spring; $p$ is the earth pressure; and $\lambda$ is a coefficient accounting for the limit displacements.

Eq. (9) can be extended to a general form, as illustrated in Fig. 5 (b). Before excavation, with the influence of the wall installation neglected, the earth pressure is equal to earth pressure at rest. Then, radial wall displacements develop during excavation, compressing or stretching the soil springs and leading to pressure increases or decreases until their limit states are reached. According to the adopted sign convention, all four hyperbolic curves can be unified into a single equation, as follows:

$$p = p_0 - \frac{u}{\frac{1}{k_i} - \lambda\frac{u}{p_u - p_0}} \tag{10}$$

where $p_0$ is the at-rest earth pressure; and $p_u$ is the active or passive earth pressure.

The earth pressure $p = p_u$ when $u$ reaches its limit value $u_u$ and can be substituted into Eq. (10) to obtain $\lambda$ using:

$$\lambda = 1 + \frac{p_u - p_0}{k_i u_u} \tag{11}$$

The comparison of a regular and revised hyperbola is shown in Fig. 6. For circular excavation, wall deflections are usually less than 50 mm. Therefore, let the passive limit displacement be 40 mm, the active limit displacement be 1/10 of the passive, and the active, at-rest and passive earth pressures be 10 kPa, 20 kPa and 50 kPa, respectively. As shown in Fig. 6, the introduction of the coefficient

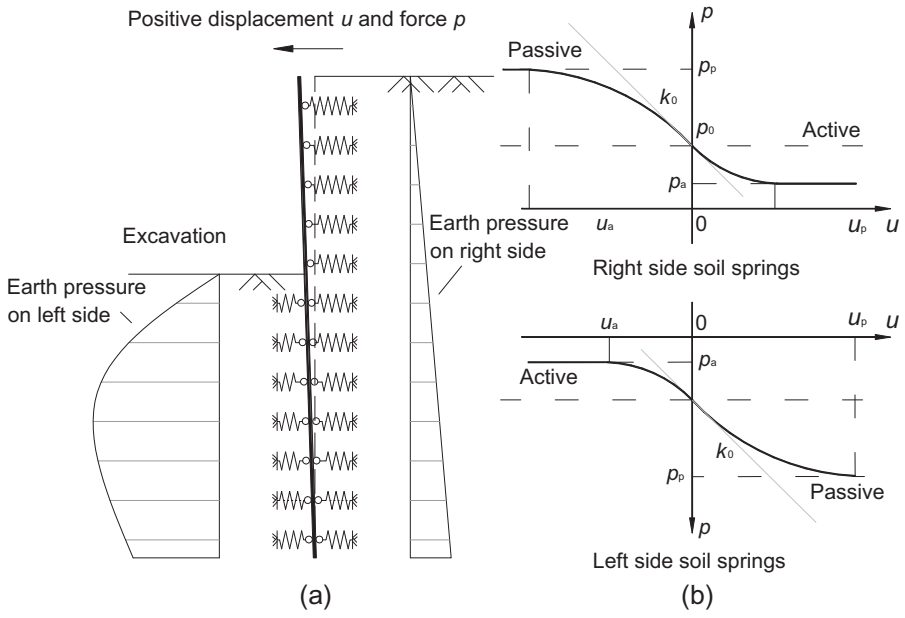


**Fig. 5.** The soil spring model on both sides of a retaining structure.

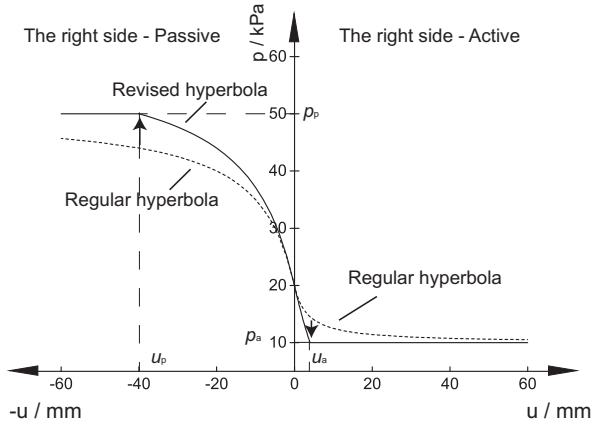


**Fig. 6.** Illustration of the soil-structure interaction model.

$\lambda$ increases the earth pressure to its limit value at a limit displacement, which more accurately describes the load-displacement characteristics of soil springs.

For a specified excavation in engineering practice, parameters such as the initial stiffness, and the active, passive and at-rest earth pressure must be evaluated for the proposed model.

### 2.3.2. Determination of parameters

The initial stiffness, $k_i$, of a hyperbolic model can be estimated based on the initial tangent subgrade reaction coefficient. The most general form of the lateral subgrade reaction modulus is [19]:

$$k_s = \alpha + \beta z^n \tag{12}$$

where $\alpha$ is a constant for vertical members; $\beta$ is the coefficient for depth variation; $z$ is the depth of interest below ground; $n$ is an exponent to give $k_s$ the best fit if load test or other data are available.

Assume that $\alpha$ is zero; we can approximate $k_s$ by using [19]:

$$k_s = \beta z = (C\gamma N_q)z \tag{13}$$

where $C$ is a constant to account for the displacement at which an ultimate earth pressure occurs; $N_q$ is the bearing capacity factor with respect to surcharge; and $\gamma$ is the unit weight of soil.

Typical values of coefficient $\beta$ are recommended in Table 1 [13]. For an assumed displacement of 0.0254 m, when the ultimate bearing pressure $q_{ult}$ is developed, $C = \frac{1}{0.0254} = 40$. Eq. (12) was proposed by Reese and has been adopted widely in engineering practice [20–22].

$N_q$ can be evaluated using [23–25]:

$$N_q = e^{\pi \tan\phi} \tan^2\left(45 + \frac{\phi}{2}\right) \tag{14}$$

The subgrade reaction coefficient can also be evaluated based on the soil properties. Vesic proposed that the subgrade reaction coefficient could be computed using the stress-strain modulus $E_s$ [26]; then, the initial subgrade reaction coefficient $k_i$ is:

$$k_i = \frac{E_i}{B(1 - v_s^2)} \tag{15}$$

where $E_i$ is the elastic modulus of soil; and $B$ is the width of the diaphragm walls.

The soil elastic modulus $E_i$ can be determined based on the shear wave velocity [27]:

$$E_i = 2\rho V_s^2(1 + v_s) \tag{16}$$

where $\rho$ is the mass density of soil; and $V_s$ is the shear wave velocity of the soil.

**Table 1**
Range of the coefficient $\beta$ for depth variation.

| No. | Soil | $\beta$ (kN/m$^4$) |
|---|---|---|
| 1 | Clayey soil ($I_L > 0.75$) | 3000–5000 |
| 2 | Clayey soil ($0.75 \geqslant I_L > 0.25$) | 5000–10,000 |
| 3 | Clayey soil ($0.25 \geqslant I_L \geqslant 0$) | 10,000–20,000 |
| 4 | Clayey soil ($I_L \leqslant 0$), coarse-grained soil, dense silty soil | 20,000–30,000 |
| 5 | Sandy soil, gravel | 30,000–80,000 |
| 6 | Dense gravel, dense coarse-grained sandy soil | 80,000–120,000 |

In addition to theoretical methods, many researchers have developed in situ technologies to assess the initial tangent coefficient. Gabr determined the initial tangent coefficient of subgrade reaction $k_i$ using a dilatometer test [28]:

$$k_i = \frac{6.5(p_0 - \sigma_h)}{half\ blade\ thickness} \tag{17}$$

where $p_0$ is the at-rest earth pressure; and $\sigma_h$ is the horizontal pressure.

After each excavation step, a layer of soil is removed, which releases the overburden stress. According to Eq. (13), the subgrade reaction coefficient decreases due to the stress release. For an excavation from depth $z_{exca,i-1}$ to $z_{exca,i}$ in a uniform soil stratum, the removed spring stiffness can be expressed by:

$$\left.\begin{array}{ll} k_i^i = \beta(z - z_{exca,i-1}) & z_{exca,i-1} < z \leqslant z_{exca,i} \\ k_i^i = \beta(z_{exca,i} - z_{exca,i-1}) & z > z_{exca,i} \end{array}\right\} \tag{18}$$

The coefficients of at-rest earth pressure, $K_0$, for sand and clay can be calculated, respectively, as follows:

Sand [29]:

$$K_0 = 1 - \sin\phi \tag{19}$$

Clay [30]:

$$K_0 = 0.19 - 0.233 I_p \tag{20}$$

The active and passive earth pressures can be obtained using Rankine's or Coulomb's earth pressure theory. Many researchers have studied the active earth pressure of circular excavation and claimed it is smaller than the plane strain pressures [31–33]. However, field test results and comparison with computed values are rare in the literature. Thus, the plane strain earth pressure theory is promising in engineering practice.

### 2.4. Ring beam behavior

Ring beams or waler beams are frequently used in circular excavations to provide more construction space. Both types of walls support a cylindrical diaphragm wall with their hoop effect. Thus, the ring beams can be simplified as distributed springs along a wall with stiffness:

$$k_{zc} = \frac{E_{zc} h_{zc}}{R_{zc}^2} \tag{21}$$

while the waler beams can be simplified as a spring connected to a wall with stiffness:

$$k_z = \frac{E_z A_z}{R_z^2} \tag{22}$$

## 3. The finite element format

Eq. (3) can be rewritten in matrix form:

$$([k_b] + [k_c] + [k_{zc}] + [k_{in}] + [k_{ex}])\{u\} = \{\Delta p_0\} \tag{23}$$

where $[k_b]$ is the beam element stiffness matrix [34]; $[k_c]$ is the equivalent spring stiffness of the hoop effect; $[k_{zc}]$ is the stiffness matrix of ring beams; $[k_{in}]$ is the soil spring stiffness matrix of the excavating side; $[k_{ex}]$ is the soil spring stiffness matrix of the external side; and $[\Delta p_0]$ is the difference in at-rest earth pressure at rest of two sides of the wall.

As shown by Eq. (23), the stiffness matrices of all the springs can be combined such that the spring stiffness is distributed linearly along a single element, as shown in Fig. 7. Thus, the linearly

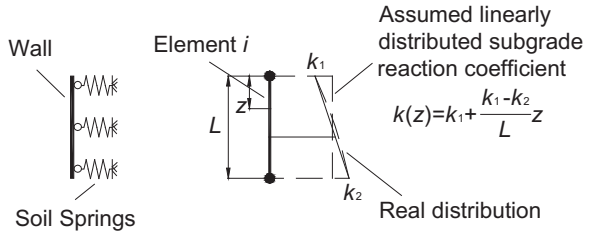


**Fig. 7.** The spring distribution.

distributed spring stiffness and external loads are general within this problem:

$$\begin{cases} k(z) = k_1 + \frac{k_2 - k_1}{l} z \\ p(z) = p_1 + \frac{p_2 - p_1}{l} z \end{cases} \tag{24}$$

The matrix of the soil stiffness and loads can be derived using the Galerkin method:

$$\int_0^L k(z) N_i N_j \, dz = \begin{bmatrix} \frac{10k_1+3k_2}{35} l & \frac{15k_1+7k_2}{420} l^2 & \frac{9k_1+9k_2}{140} l & -\frac{7k_1+6k_2}{420} l^2 \\ & \frac{5k_1+3k_2}{840} l^3 & \frac{6k_1+7k2}{420} l^2 & -\frac{k_1+k_2}{280} l^3 \\ & & \frac{3k_1+10k_2}{35} l & -\frac{7k_1+15k_2}{420} l^2 \\ & & & \frac{3k_1+5k_2}{840} l^3 \end{bmatrix} \tag{25}$$

$$\int_0^L p(z) \begin{Bmatrix} N_1 \\ N_2 \\ N_3 \\ N_4 \end{Bmatrix} dz = \begin{Bmatrix} \frac{7p_1+3p_2}{20} l \\ \frac{3p_1+2p_2}{60} l^2 \\ \frac{3p_1+7p_2}{20} l \\ \frac{2p_1+3p_2}{60} l^2 \end{Bmatrix} \tag{26}$$

An iterative algorithm is required to solve the problem because the spring stiffness varies with the wall displacement in the nonlinear spring model. The difference in the wall displacement between each two iteration steps is adopted as the convergence criterion. Assume the displacement before the $i$th excavation is $u_{i-1}$ (the displacement increase is $\Delta u_{i,1} = 0$), such the $u_{i-1}$ is used to compute the soil stiffness matrix and external load matrix at the beginning. Then, the displacement is iterated until $\Delta u_i - \Delta u_{i-1} < 10^{-6}$ m. This process is coded in a Fortran program CExca1.0, and the flowchart is shown in Fig. 8.

## 4. A case study

### 4.1. Geometry and soil profile

The southern anchorage of the Yangluo suspension bridge was studied to verify the proposed axisymmetric BNEF method. The panel division and the profile of the anchorage are shown in Fig. 9 [35]. The cylindrical diaphragm wall has a 70 m outer diameter and 1.5 m thickness, and it is supported with ring beams with a thickness of 1.5–2.5 m. The excavation was divided into 14 phases, with 3 m of soil excavated in each phase, except for the last phase, in which 2.5 m was excavated. The soil parameters of the strata are shown in Table 2, where $\beta$ is evaluated using Eq. (13) with $C = 80$.

### 4.2. Wall displacement

According to Eq. (21), the equivalent spring stiffness of the ring beams is $K_{zc} = 36.97$ MPa. The relevant stiffness reduction coefficient is 0.487, according to Eq. (8). The calculated and measured wall displacements are plotted in Fig. 10. Similar to the measured

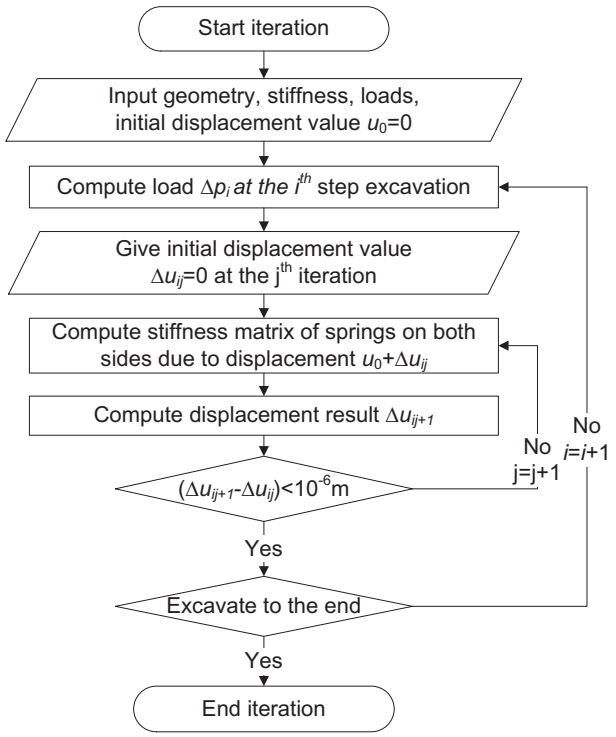


**Fig. 8.** The flowchart of the BNEF program.

values, the calculated wall displacement increases with depth until reaching its maximum and then decreases to zero. The maximum calculated and measured wall displacements were 22.6 mm and 20.9 mm, which appeared at 37.8 m and 32.6 m bgl, respectively. Overall, the axymmetric BNEF method represent the main trend of wall deflection and provides a reasonable estimation for engineering purposes. However, some measured wall deflections in the first 2 stages were negative due to construction tolerance, and the retaining structure was somewhat non-circular in the plan view. This effect cannot be considered in axisymmetrical analysis in nature. Guo [36] presented a 34.5% increase in panel radial displacement with 5% construction tolerance based on a series of finite element analyses, and this result requires further study in engineering practice.

### 4.3. Internal force and stress

The vertical moment is required to determine how many reinforcing bars should be installed in diaphragm wall panels. Fig. 11 compares the calculated and measured vertical moments. Due to a lack of information, only the maximum vertical moment along the structure is given. The calculated moment is larger than the maximum measured moment, which indicates a reasonably conservative analysis. However, the directions of the moments in the upper middle section are opposite. Additionally, the location of the maximum vertical moment shifts downward during excavation, and the increase in the maximum vertical moment is moderate, which may be due to the support of the ring beams. The vertical moment reaches its maximum value in two opposite directions, above and below the excavated level. In combination with the self weight of the diaphragm walls, the vertical stresses can be obtained to verify a design.

The hoop stress can be evaluated using Eq. (4) with the calculated wall deflections, as shown in Fig. 12. The calculated maximum hoop stress of the final phase is 9.75 MPa, compared to the measured value of 10.13 MPa. The trends of the calculated and measured hoop stresses were similar. Hence, Eq. (4) is a simple and practical way to evaluate hoop stress in a circular excavation in engineering practice.

### 4.4. Earth pressure

The earth pressure on both sides of the diaphragm wall were studied in Figs. 13–15. The finite element program can calculate the whole development process of the earth pressure. Fig. 13 shows the calculated and measured earth pressures and the theoretical estimation outside the excavation. Wall deflection developed toward the excavation such that the earth pressure decreased outside the excavation until reaching the active limit state. The measured earth pressure outside the excavation shows a slight decrease in value; thus, in the calculation, the ultimate displacement was set at 30 mm. Both the measured and calculated earth pressures fell between the vertical stress ($K_0 = 1$) and active earth pressure. Due to the lower limit displacement, the earth pressure decreased faster than the passive pressure, especially in the middle section, where the maximum deflection occurs. It should be noted that the load cells were installed before casting the concrete; thus, the initial measured pressure included that induced by concrete, which is why the measured earth pressure in the lower section was significantly larger than the calculated value.

In contrast, inside the excavation, the earth pressure increases due to wall defection towards the soil in front of the wall panels until it reaches the passive limit state. The ultimate displacement of the passive earth pressure is larger than that of the active pressure, and in this calculation, 80 mm was adopted based on the recommendations of many researchers [15]. Without measured data

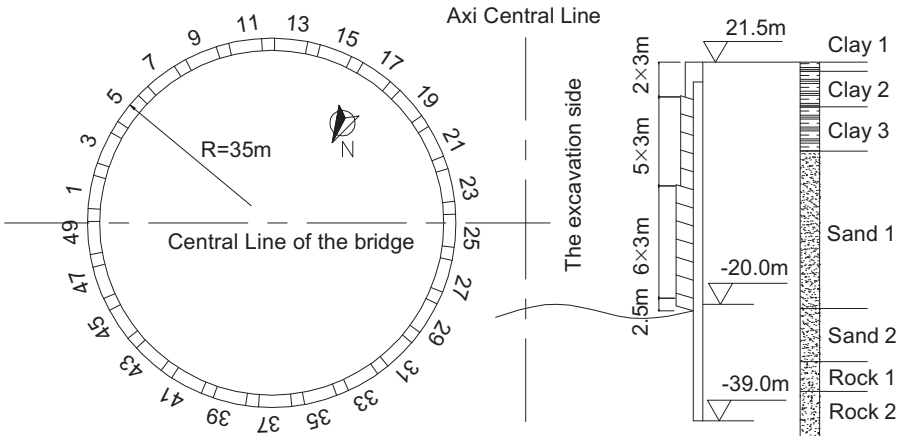


**Fig. 9.** The panel division and profile of the anchorage.

**Table 2**
Soil properties.

| No. | Soil | $\gamma$ (kN/m$^3$) | $c$ (kPa) | $\phi$ (°) | Thickness (m) | $\beta$ (kN/m$^4$) |
|---|---|---|---|---|---|---|
| Clay1 | Clayey loam | 18.5 | 12 | 10 | 1.5 | 3660 |
| Clay2 | Clayey soil | 18.2 | 10 | 8 | 6 | 3000 |
| Clay3 | Clayey loam | 18.3 | 6 | 18 | 7.5 | 7680 |
| Sand1 | Fine-grained sand | 19.2 | 5 | 32 | 26.5 | 36,000 |
| Sand2 | Gravelly sand | 20 | 6 | 40 | 9 | 103,000 |
| Rock1 | Strongly weathered rock | 20 | 20 | 55 | 5 | 1,430,000 |
| Rock2 | Weakly weathered rock | 20 | 40 | 60 | 15 | 5,100,000 |

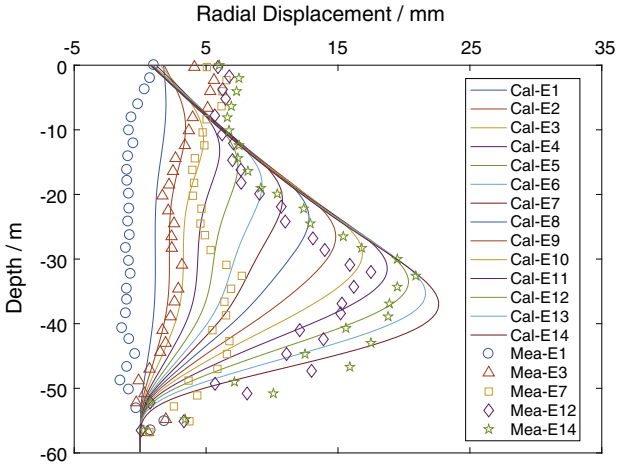


**Fig. 10.** Calculated and measured wall displacements.

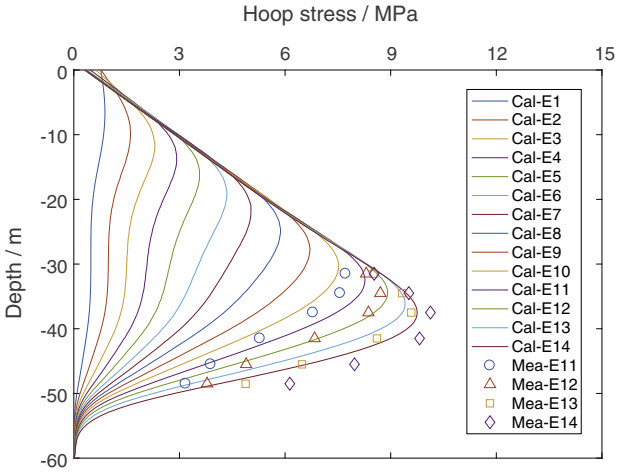


**Fig. 12.** Hoop stress in the diaphragm wall panels.

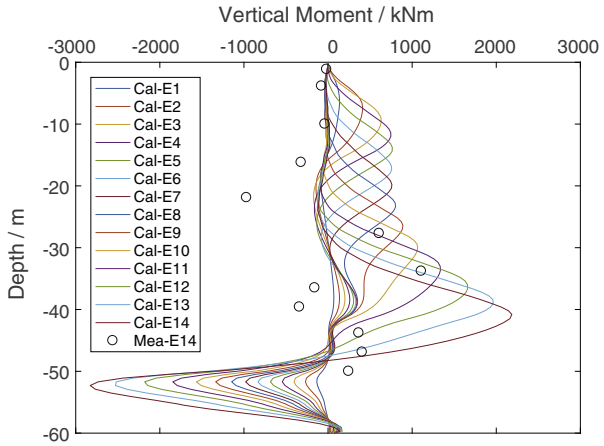


**Fig. 11.** The vertical moment of diaphragm wall panels.

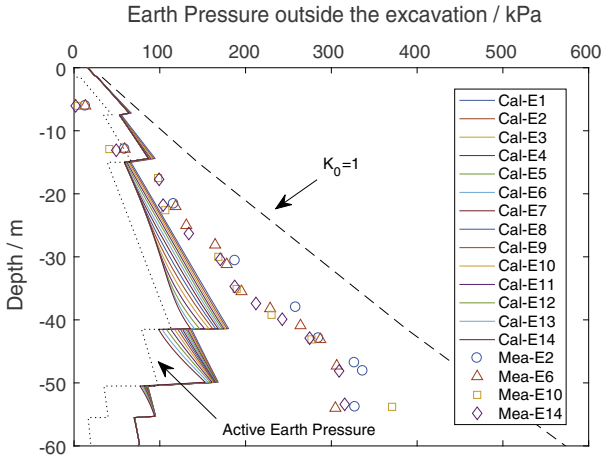


**Fig. 13.** The earth pressure development exterior to the excavation.

from the project, only the calculated and theoretical estimations are shown in Fig. 14. The earth pressure on most upper part of the wall is less than the vertical soil pressure ($K_0 = 1$), except for the lowest two layers of weathered rock. Due to excavation, the soil springs in front of the wall were partly removed on a phase-by-phase basis. This not only removed support from the excavated soils but also reduced the overburden stress acting on the soils underneath, which lowered their characteristic earth pressures. Thus, although wall displacement increased, the earth pressure did not increase monotonously. As shown in Fig. 15, the earth pressure inside the excavation at 45 m bgl increased in the first 11 phases, then decreased thereafter. We observe the same feature of pressure development at 30 m bgl, but it is less obvious. However, at the bottom of the wall, the earth pressure showed a tiny change due to the small displacement. By contrast, the earth pressure versus wall displacement relationships outside the excavation mostly showed hyperbolic curves in Fig. 15.

### 4.5. Ring beams stress

The pressure acting on the ring beams and the hoop stress were studied in Figs. 16 and 17. The radial distributed pressure is shown in Fig. 16, which indicated that the ring beams were compressed after installation, and the pressure increased along with the excavation. The maximum pressures occurred at 33 m and 36 m bgl, almost the same locations as the maximum displacement.

The hoop stress of ring beams can also be computed using Eq. (4) by substituting the radius and the Young's modulus of the ring

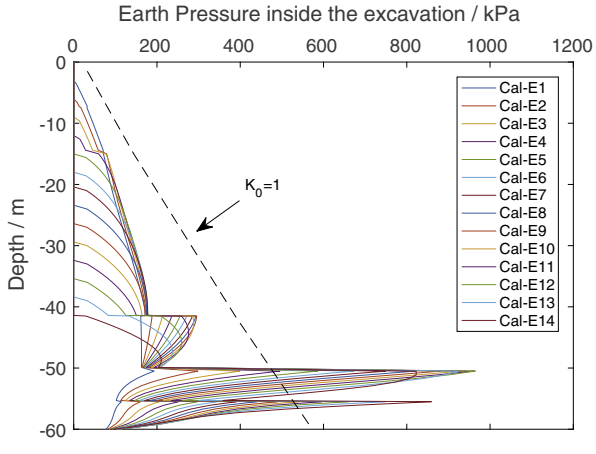


**Fig. 14.** The earth pressure development interior to the excavation.

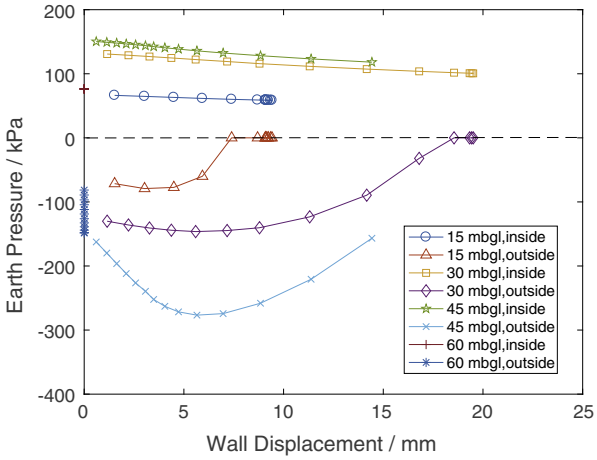


**Fig. 15.** The earth pressure vs. wall displacement.

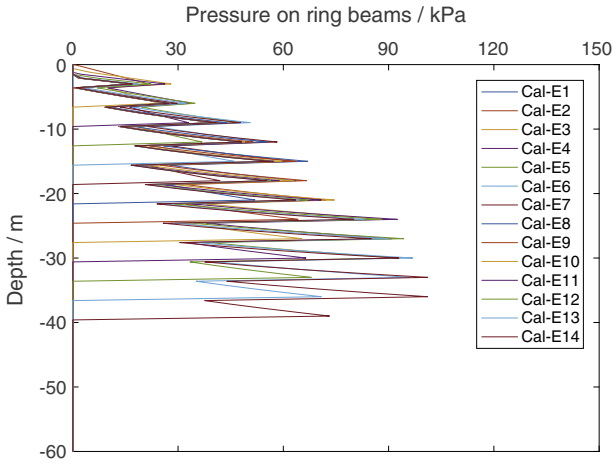


**Fig. 16.** The development of pressures on the ring beams.

beams. In Fig. 17, the hoop stress in each ring beam is plotted versus the excavation depth and is compared to the measured value. The measured hoop stresses in the ring beams are significantly higher than the calculated values, which may be due to neglecting the self weight in the calculation. Both the measured and the calculated hoop stresses are significantly less than the strength of

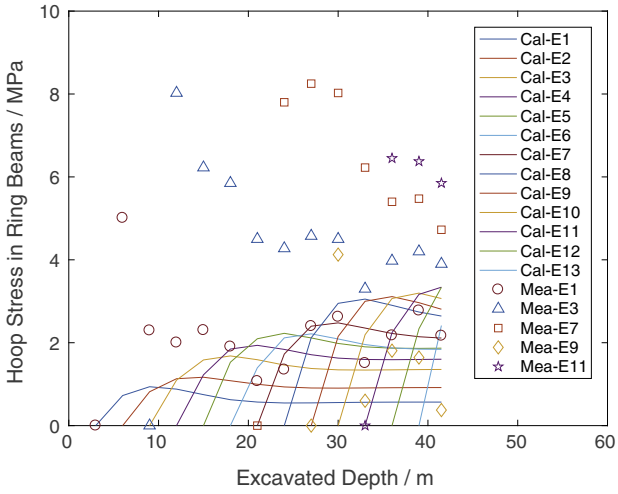


**Fig. 17.** Hoop stress in ring beams vs. excavated depth.

reinforced concrete; however, it is important to note this gap in structural design. In all ring beams, the hoop stress increased the most in the fist excavation step after installation, and the variation was less in the following steps. Thus, the lowest ring beam can be casted with slabs, and its design may be excessive. In addition, there is a peak hoop stress in each beam, after which the hoop stress decreases slightly due to the opposite displacement of the diaphragm wall. Moreover, the hoop stress remained at a low level (below 10 MPa) in the ring beams, but its construction is usually time consuming. Therefore, ring beams can be further optimized.

## 5. Conclusions

This paper has described an axisymmetric BNEF method derived from thin-shell theory to analyze circular excavations, which can provide exhaustive results for design purposes. The soil-structure interaction characteristic was introduced with nonlinear springs connected to both sides of the wall. The parameters of the spring model can be evaluated using conventional methods. Ring beams were simplified as distributed springs, and the construction sequential effect was taken into account. A nonlinear finite element solution was proposed to solve the problem, and it was verified using a real case study. The comparison indicated that the method can catch the main trend in the measured data and provide a reasonable estimation in engineering practice.

Moreover, the earth pressure development on both sides of the wall, the vertical bending moment, and the hoop stress in the ring beams were studied. The characteristics, such as the overburden stress release due to excavation, ultimate displacement, and the limit values of the earth pressures, can be considered in the program. The study also showed that the hoop stress in the ring beams remains low; thus, it could be potentially optimized in future design. The axisymmetric BNEF method is a robust and user-friendly method that could be an important alternative for the design of circular excavations.

## Acknowledgement

The financial supports provided by the China Natural Science Foundation (No. 51478051) and the Science and Technology Project on Transportation Construction by the Ministry of Communications (No. 2013318798320) are gratefully acknowledged.

## References


[1] Tan Y, Wang D. Characteristics of a large-scale deep foundation pit excavated by the central-island technique in shanghai soft clay. I: Bottom-up construction of the central cylindrical shaft. J Geotech Geoenviron Eng 2013;139(11):1875–93.

[2] Gaba AR, Simpson B, Beadman DR, Powrie W. Embedded retaining walls: guidance for economic design. London (UK): Ciria; 2003.

[3] Cabarkapa Z, Milligan GWE, Menkiti CO, Murphy J, Potts DM. Design and performance of a large diameter shaft in dublin boulder clay. In: BGA international conference on foundation – innovations, observations, design and practice. London (UK): Thomas Telford; 2003.

[4] Mcnamara AM, Roberts TOL, Morrison PRJ. Design and construction of a deep shaft for crossrail. Geotech Eng 2004;157(4):173–82.

[5] Schwamb T, Soga K. Numerical modelling of a deep circular excavation at Abbey Mills in London. Geotechnique 2015;65(7):604–19.

[6] Choi JI, Kim MM, Brandenberg SJ. Cyclic p-y plasticity model applied to pile foundations in sand. J Geotech Geoenviron Eng 2015;141(5):04015013.

[7] Tan Y. Structural behaviors of large underground earth-retaining systems in shanghai. I: Unpropped circular diaphragm wall. J Perform Constr Facil 2015;29(2):04014058.

[8] Hashash Y, Song H, Osouli A. Three-dimensional inverse analyses of a deep excavation in chicago clays. Int J Numer Anal Meth Geomech 2011;35(9):1059–75.

[9] Wang L, Luo Z, Gong W, Khoshnevisan S, Juang CH. Moment methods for assessing the probability of serviceability failure in braced excavations. In: Geo-congress 2014: geo-characterization and modeling for sustainability. p. 3293–302.

[10] Wang L, Luo Z, Xiao J, Juang CH. Probabilistic inverse analysis of excavation-induced wall and ground responses for assessing damage potential of adjacent buildings. Geotech Geol Eng 2014;32(2):273–85.

[11] Timoshenko S, Woinowsky-Krieger S. Theory of plates and shells. 2nd ed. USA: McGraw-Hill; 1987.

[12] Schwamb T, Soga K, Mair RJ, Elshafie MZEB, Sutherden R, Boquet C, et al. Fibre optic monitoring of a deep circular excavation. Geotech Eng 2014;167(2):144–54.

[13] JTG D63-2007. Code for design of ground base and foundation of highway bridges and culverts. Beijing (China): China Communications Press; 2007.

[14] BS 1881-116: 1983. Method for determination of compressive strength of concrete cubes. UK: British Standards Institute; 1983.

[15] Wilson P, Elgamal A. Large-scale passive earth pressure load-displacement tests and numerical simulation. J Geotech Geoenviron Eng 2010;136(12):1634–43.

[16] Cole RT, Rollins KM. Passive earth pressure mobilization during cyclic loading. J Geotech Geoenviron Eng 2006;132(9):1154–64.

[17] Michael DJ, Mokwa RL. Passive earth pressures: theories and tests. J Geotech Geoenviron Eng 2001;127(3):248–57.

[18] Shamsabadi A, Rollins KM, Kapuskar M. Nonlinear soil-abutment-bridge structure interaction for seismic performance-based design. J Geotech Geoenviron Eng 2007;133(6):707–20.

[19] Bowles JE. Foundation analysis and design. 5th ed. USA: McGraw-Hill; 1996.

[20] Reese LC. Laterally loaded piles: program documentation. J Geotech Geoenviron Eng 1977;103(12):287–305.

[21] Smith TD. Pile horizontal soil modulus values. J Geotech Eng 1987;113(9):1040–4.

[22] A.P. Institute. Recommended practice for planning, designing and constructing fixed offshore platforms. Washington (DC): API RP 2 A-WSD; 1993.

[23] Meyerhof GG. Some recent research on the bearing capacity of foundations. Can Geotech J 2011;1(1):16–26.

[24] Hansen JB. Revised and extended formula for bearing capacity. Earth Press 1970;28:5–11.

[25] Vesic AS. Analysis of ultimate loads of shallow foundations. Int J Rock Mech Min Sci Geomech Abstr 1900;11(11):45–73.

[26] Vesic AB. Beams on elastic subgrade and the winkler's hypothesis. In: 5th ICSMFE, vol. 1; 1961. p. 845–50.

[27] Ashford SA, Juirnarongrit T. Evaluation of pile diameter effect on initial modulus of subgrade reaction. J Geotech Geoenviron Eng 2003;129(3):234–42.

[28] Gabr MA, Lunne T, Powell JJ. P-y analysis of laterally loaded piles in clay using DMT. J Geotech Eng 1994;120(5):816–37.

[29] Jaky J. The coefficient of earth pressure at rest. J Soc Hung Architects Eng Budapest, Hungry 1944;(10):355–8.

[30] Alpan I. The empirical evaluation of the coefficient $k_0$ and $k_{0,R}$. Soils Found 1967;7(1):31–40.

[31] Cheng YM, Hu YY, Wei WB. General axisymmetric active earth pressure by method of characteristics? Theory and numerical formulation. Int J Geomech 2007;7(1):1–15.

[32] Liu FQ, Wang JH, Zhang LL. Analytical solution of general axisymmetric active earth pressure. Int J Numer Anal Meth Geomech 2009;33(4):551–65.

[33] Liu FQ, Wang JH, Zhang LL. Axi-symmetric active earth pressure obtained by the slip line method with a general tangential stress coefficient. Comput Geotech 2009;36(1–2):352–8.

[34] Smith IM, Griffiths DV, Margetts L. Programming the finite element method. UK: John Wiley & Sons Ltd; 2014.

[35] Yang Yuquan, Wu Hao, Liu Minghu. Monitoring technology and research of Wuhan Yangluo Yangtze highway bridge South Anchor deep foundation. In: The 2nd national geotechnical and engineering proceeding in China.

[36] Guo Huiguang XW, Yutao Liu. Analysis of excavation simulation and field measurements of south anchorage foundation deep pit of Yangluo Chagnjiang river highway bridge. Bridge Constr 2005(3):16–9.